



Available online at [www.sciencedirect.com](http://www.sciencedirect.com)

SCIENCE @ DIRECT®

C. R. Chimie 8 (2005) 1617–1630



<http://france.elsevier.com/direct/CRAS2C/>

Account / Revue

## Structural powder diffraction characterization of organometallic species: the role of complementary information

Norberto Masciocchi <sup>a,\*</sup>, Angelo Sironi <sup>b,\*</sup>

<sup>a</sup> Dipartimento di Scienze Chimiche ed Ambientali, Università dell'Insubria, via Valleggio 11, 22100 Como, Italy

<sup>b</sup> Dipartimento di Chimica Strutturale e Stereochimica Inorganica, Università di Milano, via G. Venezian 21, 20133 Milan, Italy

Received 29 April 2004; accepted 17 January 2005

Available online 03 May 2005

---

### Abstract

X-ray powder diffraction (XRPD) has been employed in the last years as an active structural tool, well beyond its classical usage in qualitative, quantitative and microstructural analyses. The complexity of the materials studied by this method has steadily grown, allowing the full structural characterization of molecular systems, of organic and organometallic nature. Here we emphasize that, when dealing with such moderately complex molecular materials, the power of XRPD can be enhanced not only by increasing the radiation flux or the instrumental resolution, but also (and cheaply) by using additional (experimental or computational) information. *To cite this article: N. Masciocchi, A. Sironi, C. R. Chimie 8 (2005).*

© 2005 Académie des sciences. Published by Elsevier SAS. All rights reserved.

### Résumé

La diffraction des rayons X sur poudre (XRPD) a été employée ces dernières années comme outil structural, au-delà de ses utilisations classiques dans les analyses quantitatives, qualitatives et microstructurales. La complexité des matériaux étudiés par cette méthode a crû de manière constante, permettant la caractérisation structurale complète de systèmes moléculaires de nature organique ou organométallique. Ici, nous faisons ressortir qu'en utilisant des matériaux moléculaires modérément complexes, la capacité de la diffraction des rayons X sur poudre peut être augmentée non seulement en accroissant le flux de radiation ou la résolution instrumentale, mais aussi (et à moindre coût) en utilisant des informations complémentaires de nature expérimentale ou théorique. *Pour citer cet article: N. Masciocchi, A. Sironi, C. R. Chimie 8 (2005).*

© 2005 Académie des sciences. Published by Elsevier SAS. All rights reserved.

**Keywords:** Powder diffraction; Crystal structure; Organometallic compounds; Rietveld method

**Mots clés :** Diffraction des rayons X sur poudre ; Structure cristalline ; Composés organométalliques ; Méthode de Rietveld

---

\* Corresponding authors.

*E-mail addresses:* [norberto.masciocchi@uninsubria.it](mailto:norberto.masciocchi@uninsubria.it) (N. Masciocchi), [angelo.sironi@istm.cnr.it](mailto:angelo.sironi@istm.cnr.it) (A. Sironi).

## 1. Introduction

For decades, chemists, mineralogists and material scientists have been employing powder diffraction as the most powerful (analytical and structural) method in the characterization of metals, alloys, salts, rocks and ores, i.e. of *classic inorganic* compounds. At variance, until the mid nineties, the realm of *molecular* materials (such as **organics** and pharmaceutically active species) was largely colonized by single crystal diffraction, given that their structural complexity seemed to restrict the use of powder diffraction to phase identification (which is, nevertheless, a highly profitable activity: indeed, quantification and detection of polymorphs and solvates have consequences of high economical value). Once the recent improvements in radiation sources, optics, instrumentation, detectors, computers and software were made available to the wide community of structural chemists, the derivation of a structural model for such species (*from powder diffraction data ‘only’*) came within reach [1]. Nowadays, the increase of instrumental resolution and new efforts in devising indexing algorithms make it possible to detect, even from polyphasic mixtures [2], the correct unit cell of an unknown species, and, eventually, to solve (by a combination of direct- or reciprocal-space techniques, brutal force [3], and more advanced methods [4]) their crystal *and* molecular structures. Recently, also the structures of a number of **organometallic** species and covalent **polymers** [5] have been successfully retrieved, leading to the discovery of new stoichiometries, connectivities and geometries, unforeseen [6], unexpected [7] or even badly postulated [8], throughout the years, on the basis of weak spectroscopic evidence.

The use of powder diffraction in the field of organic–inorganic hybrids (which is larger than that of simple organometallics) presents a series of problems which, being somewhat characteristic of the very nature of these species (see Fig. 1), cannot be overcome by increasing the radiation flux and the instrumental resolution, but can be only circumvented by using additional (experimental or computational) information.

Indeed:

- 1. Molecular compounds (and ‘salts’ containing *large* polyatomic ions) are bound by weak intermolecular forces, hence have high thermal parameters, large peak widths and a rapid fall-off of the scattering power with the scattering angle. A large intrinsic

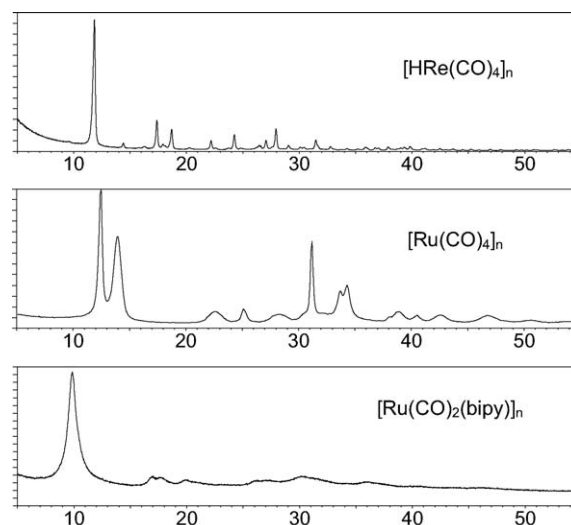


Fig. 1. Raw XRPD patterns for three 1D organometallic polymers, showing different degrees of crystallinity, and markedly anisotropic peak widths, up to  $1.5^\circ 2\theta$ .

peak width is known to hamper the indexing process (the key step in *ab initio* X-ray powder diffraction (XRPD)), while the absence of significant reflections above  $\sin\theta/\lambda = 0.4 \text{ \AA}^{-1}$  dramatically decreases the attainable resolution, leading often to uninterpretable Fourier maps (for light atoms linked by short bonds) and instabilities in the Rietveld refinement.

- 2. While solution of the phase problem is often simplified by the presence of heavy scatterers [the metal(s)], completion of the structural model is more difficult, because of the weaker contribution to the whole scattering power of light atoms, which can be then easily missed, or poorly located, in difference Fourier maps. Worthy of note, these maps suffer of a further inherent problem, in that  $|F_{\text{obs}}|$  are normally extracted (for overlapping reflections) through a partitioning algorithm based upon the already found (partial) model: this artificially lowers the pertinent  $R_{\text{Bragg}}$  and  $\Delta F$  values, thus affecting the overall quality of the difference Fourier map.
- 3. Most organometallic species contain ligands with a wide conformational flexibility, which make the different steps of structure solution, model completion and/or theoretical crystal structure predictions even more difficult.

As a consequence, the structural ‘details’ which can be obtained by powder diffraction are rather blurred; nev-

ertheless, XRPD still affords a plenty of useful, otherwise inaccessible<sup>1</sup>, information such as paracrystallinity, molecular shape, heavy atoms stereochemistry, rough bonding parameters and crystal packing. Even if these were the only attainable results, XRPD would be considered an unavoidable source of structural information and a fruitful complement to other structural techniques. However, we will show in the next pages that the joint use of multiple observations increases the power of the XRPD technique, which has been recently lead to the discovery of unforeseen crystallochemical features, well beyond the simple (geometrical) description of the solved structure.

## 2. Discussion

In the early nineties we started a project on the structural characterization of co-ordination compounds from PD data measured on conventional equipment [9], and soon realized the necessity of adding ‘external’ (i.e. not present in the diffraction pattern) information in order to improve the quality of the results, because the independent atom models often converge to unphysical bonding values. Typically, the detailed knowledge of the most common stereochemistries (available from databases) and the hidden assumption that harmonic wells (of arbitrary curvature) about ‘reference’ values can be added in a *generalized* cost function, allow to include geometrical restraints in the refinement procedure. Accordingly, the widely used programs for Rietveld refinement, in their presently available versions (May 2004), GSAS [10], Fullprof [11], Rietan [12], and TOPAS [13], *all* include a wide spectrum of possible restraints, on distances, angles, torsions, planarity and even chirality.

While the most simple geometric approximations (interatomic distances and angles) hold for intramolecular contacts, parameterization of nonbonding (*intra*- and *inter*-molecular) interactions by this technique is

<sup>1</sup> When dealing with (i) insoluble, thermally unstable, compounds which cannot be (re)crystallised from solution or from the melt; (ii) metastable phases destroyed or modified upon manipulation; (iii) twins; (iv) very small crystals and/or crystal aggregates; (v) gas/solid, liquid/solid and solid state reactions fragmenting and misorienting the coherent domains of the starting crystals but conserving the (poly)crystalline nature of the sample [9].

not viable, because the flatness of their potential energy wells and their asymptotic behavior for large separations can hardly be reproduced by restraining a number of interatomic distances. Notwithstanding, the correct structural model should correspond to a packing energy minimum and, simultaneously, be consistent with the experimental diffraction data; therefore, as briefly described in the following, we employed Energy + Rietveld (uncoupled, but iterated) refinements, in search for a valuable tool for obtaining and/or validating *ab initio* XRPD crystal structures.

### 2.1. Molecular mechanics (MM) in the crystal lattice as a tool for solving structures

While solving the crystal structure of  $[(\text{CO})_2\text{Rh}(\mu\text{-Cl})_2\text{Rh}(\text{C}_8\text{H}_8)]$ , **1** [14] (see Fig. 2) location of two crystallographically independent Rh atoms (Patterson) and two bridging Cl ions (difference Fourier) was easily achieved. At this point, although the Rh(I) atoms were likely in square planar environments (an  $\eta^2$ -ligand simulating a single donor site), no easily distinguishable C and O atoms (of the carbonyl or cyclooctadiene ligands) could be found in a further difference map. However (unconventionally) resorting to packing considerations, i.e. to the qualitative analysis of the empty volumes about the  $\text{Rh}_2\text{Cl}_2$  core, we clearly detected which metal was bound to cyclooctadiene and which to carbonyls.

Therefore, the location and orientation of the chelating diolefin were initially determined by *rough* standard molecular building procedures (performed by SMILE [15]); this step, in which the  $\text{C}_8\text{H}_8$  fragment was attached to the pertinent metal atom in a very approximate conformation (and disregarding the crystal environment), was followed by a steric energy minimization of the whole *flexible* molecule within its crystal lattice (thanks to a locally developed program [16]), which eventually afforded a good starting point for the

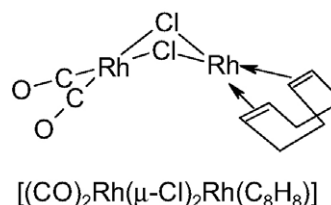


Fig. 2. Schematic drawing of the roofed structure of  $[(\text{CO})_2\text{Rh}(\mu\text{-Cl})_2\text{Rh}(\text{C}_8\text{H}_8)]$ .

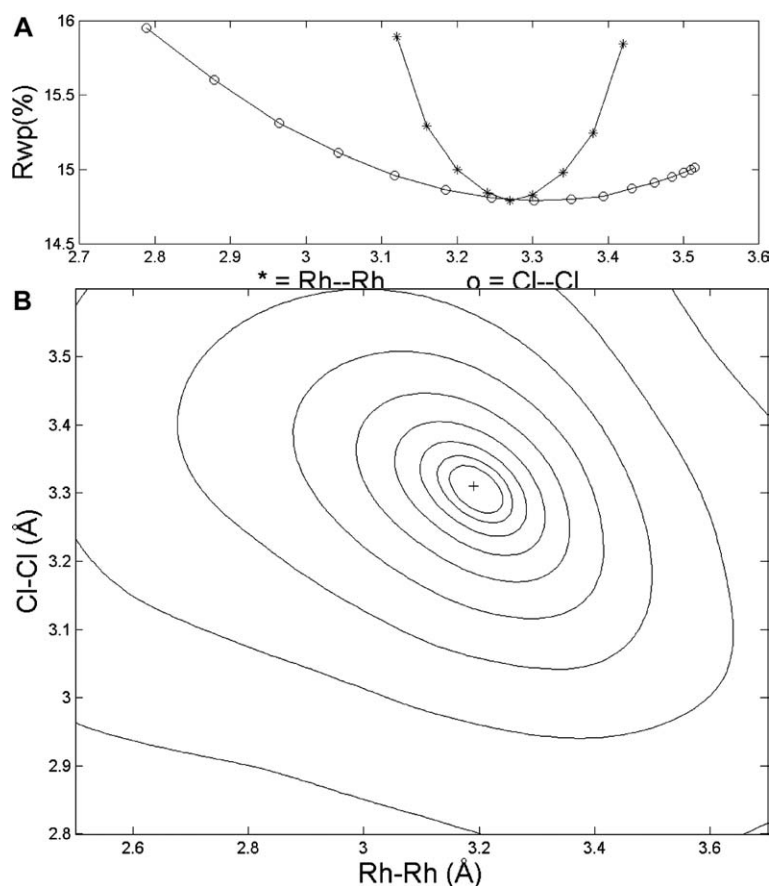


Fig. 3. Top: Monodimensional cuts of the  $R_{wp}$  hypersurface along the Rh...Rh and Cl...Cl directions, respectively. Bottom: 3D view of the potential energy hypersurface, projected onto the Rh...Rh vs. Cl...Cl plane (values in Å).

final (restrained) Rietveld refinement ( $R_p$  and  $R_F = 0.116$  and  $0.085$ , respectively).

Finally, the roof-shape of the  $Rh_2Cl_2$  fragment and the overall feasibility of Rietveld/MM refinements were checked by comparing the (two) *one-dimensional* cuts of  $R_{wp}$  (along the Rh...Rh and Cl...Cl directions, respectively) with the two-dimensional section (Rh...Rh/Cl...Cl) of the potential energy hypersurface, PES (see Fig. 3). Interestingly, but not exceptionally, even if the minima of the two independent cost functions are close (which is not always true),  $R_{wp}$  is much more sensible to high  $Z$  atoms (Rh vs. Cl) displacements, while the PES is softer along the Rh...Rh direction than along Cl...Cl. As a direct consequence, joint refinements should face the non-trivial problem of relative scaling of different ‘observations’ which, at present, is not uniquely defined.

## 2.2. MM in the crystal lattice as a tool for validating structures

A ‘standard’ ab-initio XRPD structure determination of  $\{(phen)Pd[C(=O)ON(-CH_3)C(=O)]\}_2$  (phen = 1,10 phenanthroline) [17], was undertaken to determine the controversial [18] connectivity pattern of this complex organometallic species. Briefly: (i) peak search and indexing of data collected on a conventional powder diffractometer afforded an orthorhombic unit cell of approximate dimensions  $a = 7.09$ ;  $b = 10.66$  and  $c = 17.27$  Å, space group  $Pna2_1$ ,  $Z = 4$ ,  $M(24) = 17$ ,  $F(24) = 33$  (0.013, 57); (ii) interpretation of the Patterson map allowed location of the unique Pd atom; (iii) the lack of a center of symmetry and what was later interpreted as a remarkable preferred orientation determined a noisy and not easily interpretable differ-

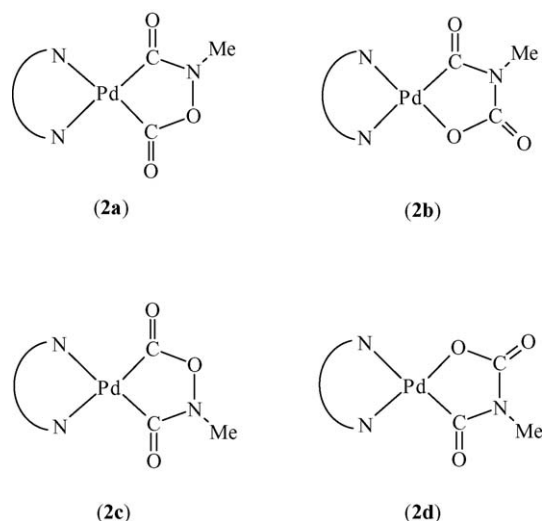


Fig. 4. Possible stereoisomers of species **2**. Note that the (**2a**, **2c**) or (**2b**, **2c**) couples represent crystallochemically, not *chemically*, distinct 'isomers'.

ence Fourier map; (iv) the orientation of a planar (phen)Pd<sub>2</sub> fragment was determined by a rotational grid search about the (refinable) Pd atom position, using P-RISCON [19] and optimized by a rigid-body Rietveld refinement, using a Z-matrix formalism implemented by us into a local version of the program PREFIN [20] (now incorporated into DEBVIN [21]); (v) completion of the structure with the few missing light atoms was possible by a surprisingly informative difference Fourier map (see Fig. 5) obtained on newly collected data free of texture effects; (vi) the correct stereoisomer (**2a** in Fig. 4) was clearly identified by the position of the missing substituent in the metallacycle.

The relevant stereochemical task of this structural study was to discriminate between two different stereoisomers of **2**, each one possibly occurring in the crystal in two different orientations (see Fig. 4); therefore, a cross-validation of the XRPD results (structure **2a**) was achieved by MM [16].

Given the significantly different energy values reported in Table 1, our computations differentiated among the four plausible structures depicted in Fig. 4, reinforced the XRPD results and showed that subtle information of the molecular shape, hidden in the lattice metrics, symmetry operations and heavy atom locations (obtained from XRPD without a priori information), can successfully be retrieved by MM. Note that, given the quality of the Fourier map in Fig. 5, this vali-

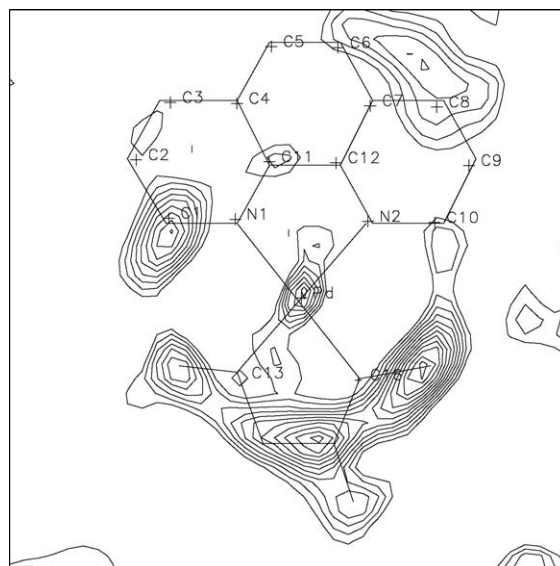


Fig. 5. Difference Fourier map in plane with the Pd(phen) moiety (sketched by thin straight lines); the residual electron density clearly indicates which of the *four* moieties (**2a**) was present in the crystal of **2**.

Table 1  
Results of the steric energy computations (kcal mol<sup>-1</sup>) for molecules **2a–2d**

Fragment (as in Fig. 4)	<b>2a</b>	<b>2b</b>	<b>2c</b>	<b>2d</b>
Total steric energy, SE <sub>i</sub>	-24.0	-17.4	+26.6	+7.1
Intramolecular energy, IE <sub>i</sub>	+25.2	+25.4	+38.5	+35.0
Packing energy, PE <sub>i</sub>	-49.2	-42.8	-11.9	-27.9
SE <sub>i</sub> -SE <sub>2a</sub>	0.0	+6.6	+50.6	+31.1

dation may appear redundant. However, because the original textured data did not allow the successful completion of steps (v) and (vi), we actually employed MM *well before* resynthesizing our product. It was indeed this *computational* evidence which stimulated us to attempt such difficult synthesis again, in search for a less textured sample.

### 2.3. MM in the crystal lattice as a tool for incorporating 'previous stereochemical knowledge'

Here we discuss the structures of three organometallic polymers [22]<sup>2</sup>, namely [ReH(CO)<sub>4</sub>]<sub>n</sub> [23]

<sup>2</sup> One-dimensional and 'pseudo' one-dimensional materials have since long fascinated physicists and chemists because of their unusual properties. There is a recent renaissance of research in the area of 1D polymers with metal-containing backbones possibly in the light of the explosion of interest in nanoscale electronic devices.

$[\text{Ru}(\text{CO})_4]_n$  [24] and  $[\text{Ru}(\text{CO})_2\text{bipy}]_n$  [25] (bipy = 2,2'-bipyridine) for which the representative XRPD patterns have been presented above in Fig. 1.

In all three cases there are two kinds of problems which are deeply entangled: (i) the structural complexity of the materials, for which XRPD alone is not able to afford accurate atomic positions, particularly when strong scatterers are present (Re, Ru), and (ii) the sample contribution, which is a clear manifestation of the presence of defects, inherent in the actual phase. Interestingly, and at variance from conventional single crystal studies, XRPD affords, in some cases, some extra-information of microstructural parameters, such as strain and coherence lengths, which are normally overlooked.

The analyses of the XRPD traces of very different 'quality' (as shown above) clearly resulted in structural models of different accuracy; modeling and geometrical restraints were necessary in the first two cases to help convergence in the final Rietveld refinement cycles; differently, the very limited amount of information present in the bottom trace of Fig. 1 required the knowledge of the previously determined ruthenium tetracarbonyl structure in order to assess the few 'accessible' structural features (cell parameters hence crystal

packing) of the ruthenium polymers containing diaz-aaromatic ligands.

In the first of our examples, the  $[\text{HRe}(\text{CO})_4]_n$  polymer, the three crystallographically independent metal atoms, each one defining its own infinite  $3_1$  (homo-chiral) helix, were unambiguously located by Direct Methods (EXPO [26]); however, due to the intrinsic limitations of XRPD, we were unable to complete the starting model by Fourier methods; thus, we had to rely on MM and on some previous stereochemical knowledge to complete the whole structure. It is of particular interest that the preliminary information afforded by powder diffraction (i.e. lattice constants, space group symmetry and 'good' heavy atom locations) *uniquely* determine the shape of the 'cavity' containing the molecule, and, hence, the overall stereochemistry of the polymer (see Fig. 6). Finally, even the hydrogen locations were assessed (within the helical metal cores, screened by the carbonyl ligands).

In this species, as well as in the related  $[\text{HRe}(\text{CO})_4]_6$  hexamer (also solved ab initio from XRPD data), it might be considered odd to speak about hydrogen locations when we barely see the metal centers; however, it is well known that the location of the hydrides may be

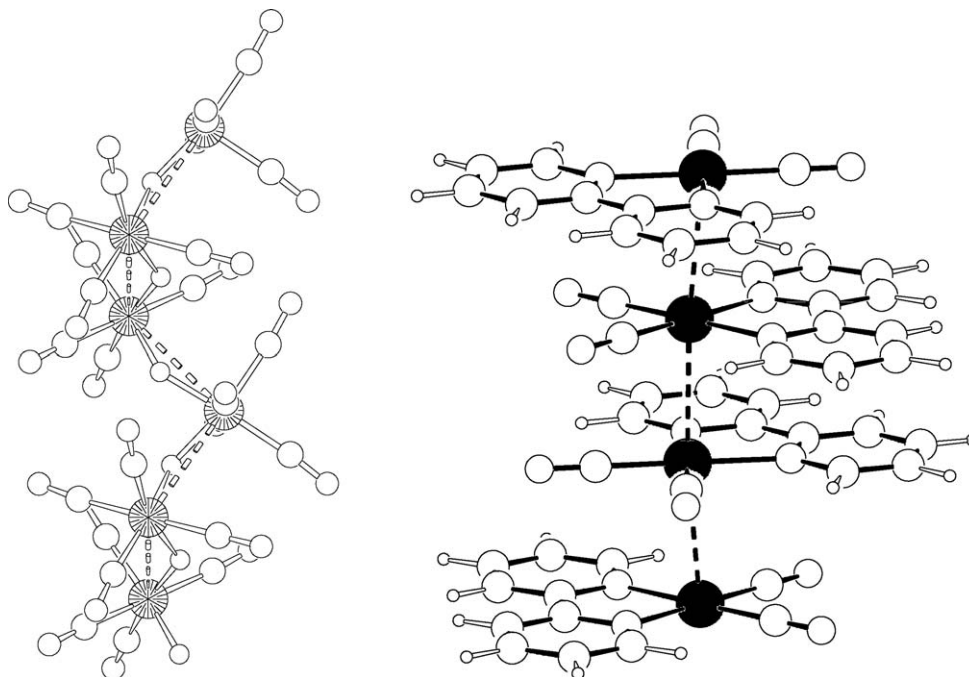


Fig. 6. Left: A fragment of the  $3_1$  helix of  $[\text{HRe}(\text{CO})_4]_n$ . Rhenium atoms as large circles. Right: Stacking of staggered  $\text{Ru}(\text{CO})_2(\text{bipy})$  fragments in the 1D polymer (for the crystal disorder, see text).

determined, at the molecular level, from those of the other atoms [27].

Among the first efforts we spent in the field of powder diffraction characterization of organometallic polymers, the determination of the crystal structure of  $[\text{Ru}(\text{CO})_4]_n$  holds a specific role: from its rather poorer XRPD trace (see Fig. 1), we still managed to determine its crystal and molecular structure, which was unexpectedly different from that guessed by IR spectroscopy [28]: instead of a zig-zag polymer built by *cis*- $C_{2v}$  fragment, linear chains, containing the staggered, *trans*  $D_{4h}$  monomers (with Ru atoms 2.94 Å apart) were found. In addition, its microstructural analysis allowed the determination of the average chain length (ca. 150 monomers) and of the lateral strain induced by the pseudohexagonal packing of parallel polymeric rods.

The structural features determined for  $[\text{Ru}(\text{CO})_4]_n$  significantly helped in unravelling the nature, and the crystal packing, of the nearly amorphous  $[\text{Ru}(\text{CO})_2(\text{bipy})]_n$  polymer, an efficient catalyst for electrochemical carbon dioxide reduction and water gas shift reaction [29]. In this case, we had to ‘manually’ guess the lattice parameters by observing the systematicity of the  $d^*$  ratios of the few observable bumps, as well as by detecting their subtle splitting.

Once the correct cell and lattice centering were detected, model building and allowance for an extremely (but, eventually, easily interpretable) disordered structure allowed a rather decent, yet unexpected, matching between the observed and calculated XRPD traces. The final model confirmed the polymeric nature of the sample, which shows stacking of  $C_{2v}$ - $\text{Ru}(\text{CO})_2(\text{bipy})$  fragments (ca. 3.0 Å apart), staggered (by  $\pm 45^\circ$  or  $\pm 135^\circ$ , as in the parent  $[\text{Ru}(\text{CO})_4]_n$ ), but disordered in *four equivalent orientations* about  $z$ .

#### 2.4. Selected area electron diffraction (SAED) as a tool for indexing large cells

Two-dimensional systems are common to many aspects of material chemistry. The variety of the available organic ligands (and the tendency of certain inorganic substrates to afford well defined layers) can be used to design low-dimensional hybrid inorganic-organic systems with a high stereochemical control, exploiting (strong) covalent bonding, weaker dipolar effects, segregation or intercalation processes.

The crystal morphology of Magnetic Cobalt Soaps, as shown in Fig. 7, clearly shows that, more than ever,

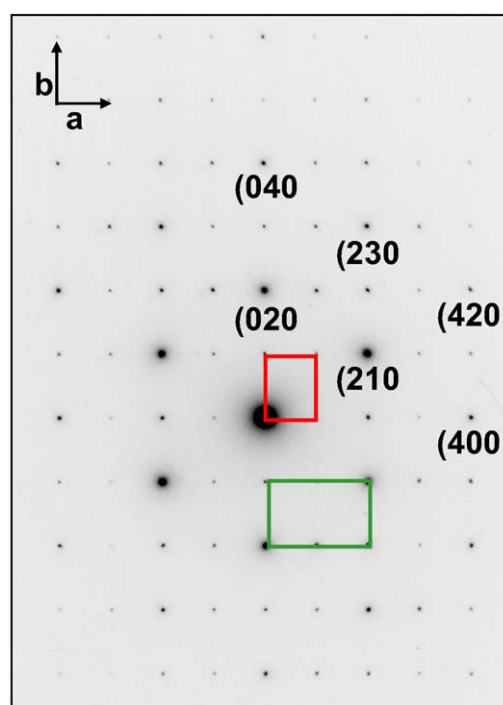
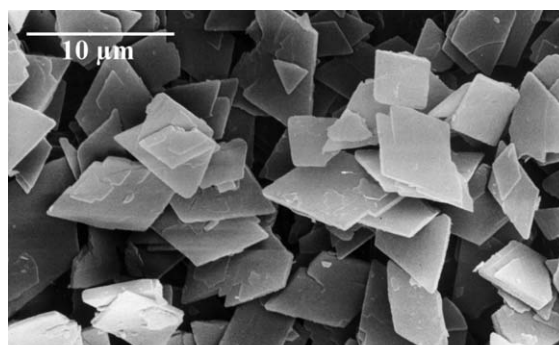


Fig. 7. Top: Crystal morphology of *cis*- $\text{Co}(\text{H}_2\text{O})_2(\text{C}_{20}\text{H}_{39}\text{O}_2)_2$ , from SEM micrographs. Bottom: characteristic electron-diffraction pattern as recorded with the platelets oriented perpendicularly to the electron beam. The rectangles correspond to the ( $a^*$ ,  $b^*$ ) cell of the present compounds (small) and of the paraffin-like subcell (large).

preferential orientation effects are likely at work. This is a rather annoying problem, both in the indexing, but particularly in the structure solution (and refinement) stages. Nevertheless, careful sample preparation<sup>3</sup>, the

<sup>3</sup> If possible, the side-loading technique should be used (H.F. Mc Murdie, M.C. Morris, E.H. Evans, B. Paretzkin, W. Wong-Ng, Powder Diffr. 1 (1986) 40), unless only a small quantity of material is available (in such case, the capillary mounting is desirable).

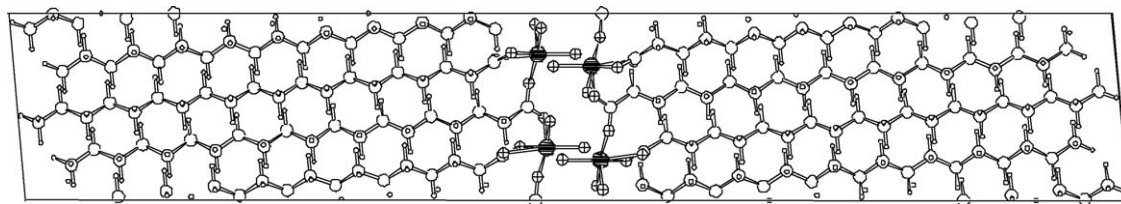


Fig. 8. Schematic plot (down  $b$ , horizontal axis =  $c$ ) of the crystal structure of  $cis\text{-Co}(\text{H}_2\text{O})_2(\text{C}_{20}\text{H}_{39}\text{O}_2)_2$ , showing the elongated organic ligands running nearly parallel to the  $c$  axes; cobalt atoms in black, oxygen atoms cross-hatched.

use of a highly monochromatized soft radiation ( $\text{Co-K}\alpha_1$ ), and particularly the metric information gathered from SAED on a single platelet (Fig. 7, bottom) allowed the structural analyses of a number of (monoclinic) cobalt soaps with cell parameters as large as  $58 \text{ \AA}$ . Due to their structural complexity, neither direct nor Patterson methods afforded unique (refinable) cobalt atom locations, that could be later used for model completion by Fourier methods. However, direct space *simulated annealing* techniques, using two independent rigid *all-trans* alkanolate groups and one *cis*- $\text{Co}(\text{H}_2\text{O})_2$  fragment, eventually afforded reasonable starting models. Thus, coupling SAED with tailored XRPD measurements, we successfully characterized a number of mono- and dicarboxylato(diaqua)cobalt(II) species [30].

These compounds belong to the same structural class, with long chain organic ligands segregated from the polar heads and metal ions connected by  $\text{RCO}_2$  bridges in the rare *anti-anti* conformation (see Fig. 8). Based on the structures determined from XRPD data, the interpretation of the low-temperature magnetic behavior and of the coupling constants of a two-dimensional magnetic lattice was then possible.

### 2.5. Merging optical and structural data into a comprehensive structural model

$[\text{DAMS}^+][\text{Cu}_5\text{I}_6]$  ( $[\text{DAMS}^+] = [\text{trans-4-(4-dimethylaminostyryl)-1-methylpyridinium}]$ ) has a very simple XRPD pattern corresponding to a rather elongated rhombohedral lattice ( $a = 4.25$ ,  $c = 38.24 \text{ \AA}$ ), with approximate cell volume of  $600 \text{ \AA}^3$ , the asymmetric unit of which cannot obviously host the large  $[\text{DAMS}^+]$  cation. What conventional diffraction sees is the stacking (along the trigonal axis with a spacing of ca.  $12.75 \text{ \AA}$ ) of  $\text{CuI}$  slabs formed by two parallel slightly corrugated sheets (similar to those present in the room temperature  $\gamma\text{-CuI}$  phase, but with a certain amount of

$\text{Cu}^{\text{I}}$  vacancies in order to balance the charges of the *guest* anions) which are suitably translated in order to grant the tetrahedral co-ordination of the  $\text{Cu}^{\text{I}}$  ion. The ‘empty’ space within the slabs (*per slab, per unit cell*) is  $96 \text{ \AA}^3$ . This implies that each  $[\text{DAMS}^+]$  cation (estimated volume  $262 \text{ \AA}^3$ , length ca.  $17 \text{ \AA}$ ) extends over three contiguous unit cells, does not conform to any translational or point symmetry operator of the host lattice, does not actually contribute to Bragg intensities except for low angle  $00\ell$  reflections and *cannot be detected in the XRPD experiment*<sup>4</sup>. Nevertheless, by coupling structural, optical and spectroscopic information we were able to suggest (see Fig. 9) that, within two *host* Cu-defective slabs, the intercalated  $[\text{DAMS}^+]$  cations must be: (i) ‘edge-on’ oriented (the interslab spacing being  $12.75 \text{ \AA}$ ); (ii) dipole ordered (given the observed SHG activity); (iii) densely packed (as J-aggregates, given the red-shifted visible absorption band); but iv) translationally disordered (given the lack of supercell  $hk0$  reflections). Finally, we were also able to propose a physical explanation for the highly crystalline rhombohedral stacking of the *host* lattice by observing that anion alignment of adjacent slabs must be due to favorable coupling of charges  $(\Gamma^-)(^{\oplus}[\text{DAMS}^+](^{\oplus})(\Gamma^-)$  originated by the substantial bilateral symmetry of  $[\text{DAMS}^+]$  nearby the charged N atom. Actually, the crucial factor controlling the formation of a macroscopic ordering is the intrinsic polarity of the ‘first’  $[\text{DAMS}^+]$  *guest* layer, which imparts a definite ‘order’ to the *host* vacancies and, simultaneously, determines the orientation of the next *guest* add-layer.

<sup>4</sup> Note that a single crystal structure determination would not perform better in this respect, since diffraction, in the presence of disordered vacancies and cations, can at most observe the averaged *host* lattice.

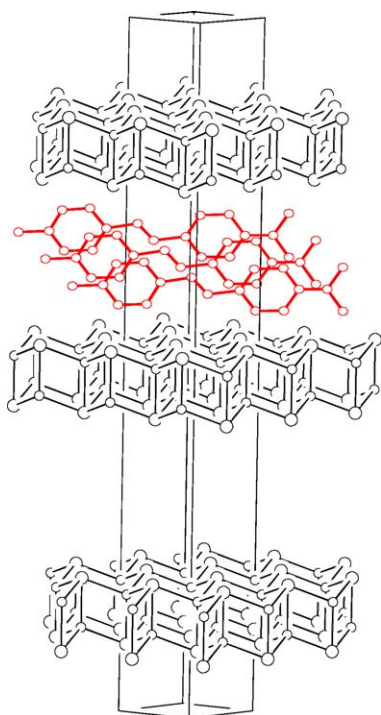


Fig. 9. Unit cell diagram for  $[\text{DAMS}^+][\text{Cu}_5\text{I}_6]$  (or  $\text{DAMS}^+@CuI$ ), showing the defective (see text)  $\text{CuI}$  layers and the intercalated  $\text{DAMS}^+$  ions. The latter are edge-on, with respect to the layers, and translationally disordered over three adjacent cells.

### 2.6. Merging neutron and X-ray diffraction data to obtain a superior structural model

$[(\mu_3\text{-H}_4)\text{Re}_4(\text{CO})_{12}]$ , **3**, is unusual among metal cluster compounds, being one of the few known ‘unsaturated’ carbonyl clusters (56 vs. 60 cluster valence electrons) [31]; its conventional X-ray single crystal structure has been previously reported by Wilson and Bau [32] and the  $\mu_3\text{-H}$  character inferred from local stereochemical considerations and an ‘image-enhanced’ (i.e. symmetry-averaged) difference Fourier map (estimated average  $\text{Re-H}$  1.77 Å). However, while studying the reactivity of solid **3** with gases ( $\text{NH}_3$ ,  $\text{CO}$  and  $\text{H}_2\text{O}$ ), using XRPD we observed a new ‘pseudopolymorphic’  $\mathbf{3}\cdot 2\text{C}_6\text{D}_6$  crystal phase, isomorphous with  $\text{Re}_4(\text{CO})_{12}(\mu_3\text{-OH})_4\cdot 2\text{C}_6\text{H}_6$  [33]. The availability of sizeable amounts of this new phase (but *not* of large single crystals) and our experience with XRPD on co-ordination and organometallics systems prompted us to attempt the viability of a new approach to hydrides location where: (i) the burden of the structure determination lies on a single crystal X-ray experiment; (ii)

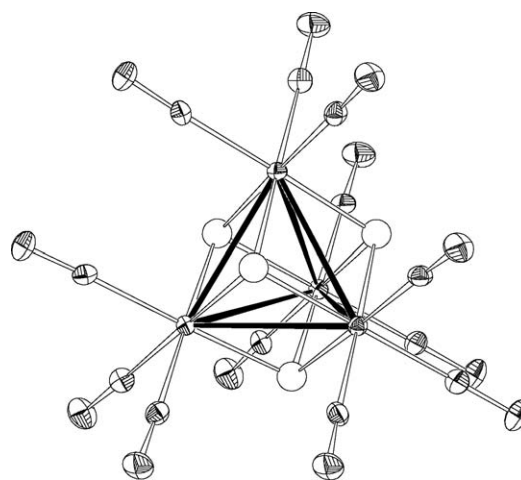


Fig. 10. Drawing of the  $[(\mu_3\text{-H}_4)\text{Re}_4(\text{CO})_{12}]$  molecule, **3**, as found in the  $\mathbf{3}\cdot 2\text{C}_6\text{D}_6$  crystal phase. The Hn atoms (see text and <sup>6</sup>) are drawn as white circles.

the accurate location of the hydrides are essentially rescued from *neutron powder diffraction*; and (iii) the final structural parameters are obtained from a *joint refinement* [34]<sup>5</sup>.

Eventually we demonstrated that  $(\mu_3\text{-H}_4)\text{Re}_4(\text{CO})_{12}$  in  $\mathbf{3}\cdot 2\text{C}_6\text{D}_6$  has a crystallographically imposed  $T_d$  symmetry (see Fig. 10), with a  $\text{Re}_4(\text{CO})_{12}$  core virtually identical to that found in **3** and confirmed the  $\mu_3$ -nature of the hydrido ligands; however, we observed significant differences in the H bonding parameters ( $\text{Re-Hx}$  1.88(12) vs. 1.77 Å,  $\text{Re-Hn}$  1.99(2) Å), where Hx and Hn labels address the ‘X’ and ‘N’ components of the *split* H atom <sup>6</sup>.

<sup>5</sup> A similar approach has been used for the analysis of the cation distribution in doped  $\text{KTiOPO}_4$  (S.J. Crenell, J.J. Owen, C.P. Grey, A.K. Cheetham, J.A. Kaduk, R.H. Jarman, J. Mater. Chem. 1 (1991) 113) and of the incommensurately modulated structure of  $\text{Bi}_2\text{Sr}_2\text{CaCu}_2\text{O}_{8+y}$  (Y. Gao, P. Coppens, D.E. Cox, A.R. Moodenbaugh, Acta Crystallogr. A49 (1993) 141). The combined use of X–N data from either two single-crystal datasets (F.A. Cotton, L.F. Chen, A.J. Schultz, C. R. Acad. Sci. Paris, Ser. II 323 (1996) 539) or two powder-diffraction experiments (R.E. Morris, W.T.A. Harrison, J.M. Nicol, A.P. Wilkinson, A.K., Cheetham, Nature 359 (1992) 519 has also been reported).

<sup>6</sup> A split atom model was used to refine the  $\mu_3\text{-H}$  atoms by invoking two ‘new’ elements,  $\text{H}_x$  and  $\text{H}_n$ , with null contribution to the N and X structure factors, respectively. This makes, inter alia, their locations substantially insensitive to the intrinsic overweight of the X dataset (in terms of quality and, perhaps, number of observations).

### 2.7. Using NMR information to drive XRPD toward the correct solution

The first efficient low voltage driven organic light emitting devices (OLEDs), reported by Tang and Van Slyke [35], were based on  $\text{Alq}_3$ . Fifteen years later,  $\text{Alq}_3$  is still a key compound widely investigated and used in electroluminescent devices. The class of tris-chelate oxyquinoline octahedral metal complexes ( $\text{Mq}_3$ ), of which  $\text{Alq}_3$  is a member, may exist in the *fac* or *mer* isomeric forms, of  $C_3$  and  $C_1$  symmetry, respectively. *Mer*- $\text{Alq}_3$  crystallizes in the  $\alpha$  and  $\beta$  phases (and in a

number of clathrates), whose optical properties are determined by the nature of  $\pi$ - $\pi$  intermolecular contacts (the shorter the contacts, i.e. the denser the crystal, the more the fluorescence is red-shifted) [36]. The first report proving the existence of *fac*- $\text{Alq}_3$  appeared in 2002 [37] and was immediately followed by other topical publications [39–41]. Noteworthy, the ‘discovery’ of the *fac*-isomer was perhaps delayed by the fact that  $\text{Mq}_3$  species were invariably found in *mer* stereochemistry, as extensively documented in [38].

$\alpha$ - $\text{Alq}_3$  polycrystalline powders can be easily transformed into a so called  $\gamma$  phase upon heating at ca

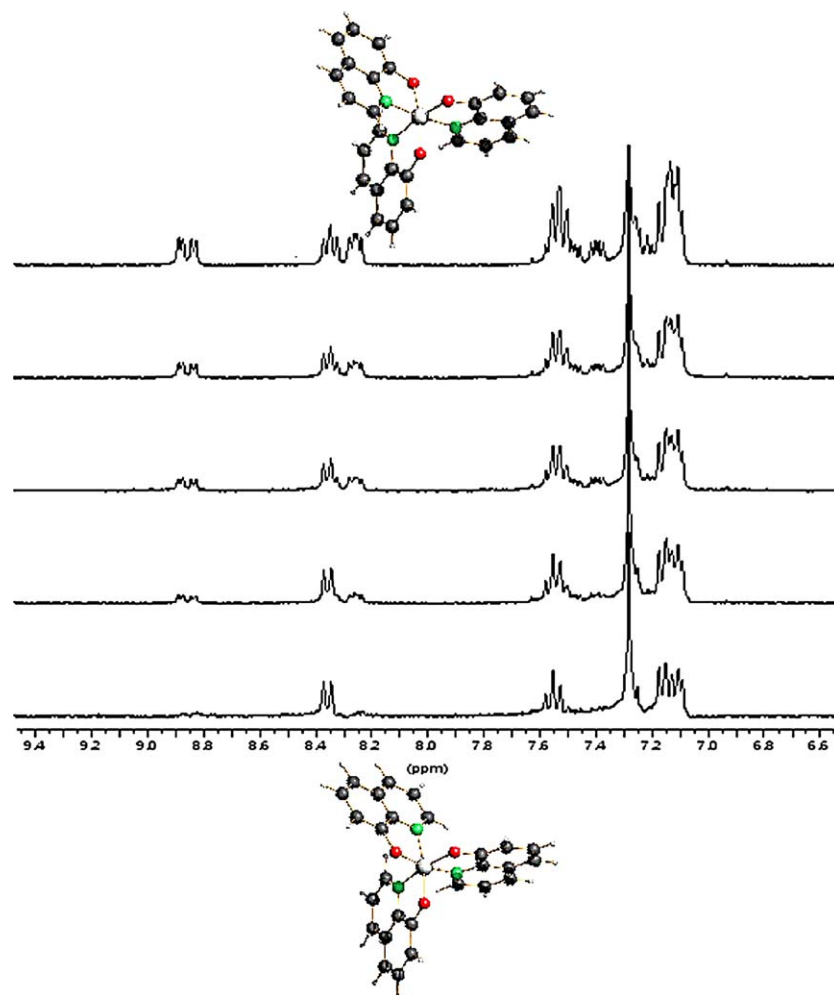


Fig. 11. Time-evolution of the  $^1\text{H}$  NMR spectra (6.5–9.5 ppm range) of  $\delta$ - $\text{Alq}_3$  dissolved in  $\text{CDCl}_3$  at  $-50^\circ\text{C}$ , measured at  $-10^\circ\text{C}$ . Bottom to top:  $t = 0, 20, 40, 60, 120$  min. Initially, the absence of ‘unperturbed’  $\text{H}_2$  signals (near  $\delta$  8.9 ppm), coupled with the fact that only the signals of three magnetically equivalent  $\text{H}_4$  nuclei are observed, shows that only the *fac*-isomer (bottom) is present. After a while, peaks of the *mer* isomer (top trace) progressively appear. The increase of the overall proton resonance intensities observed during isomerization is due to the higher solubility of *mer*- $\text{Alq}_3$  leading to a progressive dissolution of some ‘floating’ *fac*- $\text{Alq}_3$ .

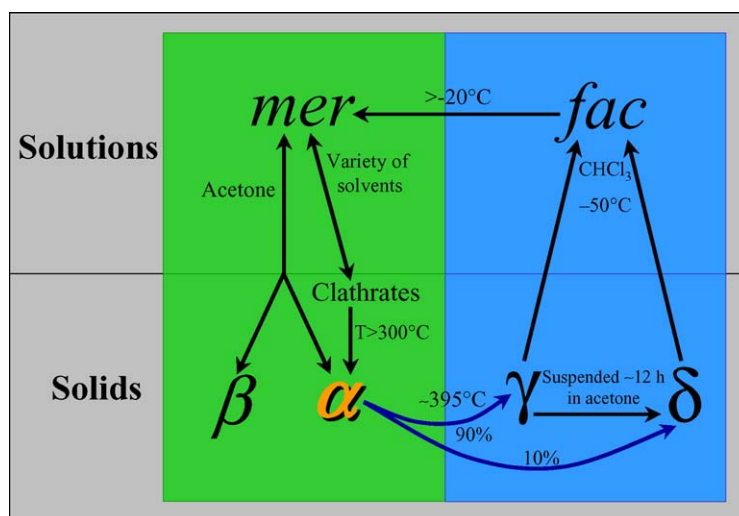


Fig. 12. Phase transformation diagram of the four distinct solid phases of unsolvated Alq<sub>3</sub> based on two different geometrical isomers. The fac-isomer can only be obtained by a solid-state reaction (blue arrows). However, dilute solutions of the fac-isomer can be prepared from the  $\delta$  (or  $\gamma$ ) phase at low temperatures, since it is kinetically stable in solution below  $-20$  °C.

400 °C under atmospheric pressure [36], while ‘train’ sublimation leads to, among others fractions, the blue emitting  $\delta$  phase, originally suggested to contain the fac-Alq<sub>3</sub> isomer [41]. Notably the  $\delta$  phase can be *quantitatively* obtained by suspending  $\gamma$ -Alq<sub>3</sub> in a few drops of liquid acetone (at RT); in addition, the observation that seeding of supersaturated mer-Alq<sub>3</sub> solutions with  $\gamma$  (or  $\delta$ ) nuclei does not yield the  $\delta$  phase, suggests that  $\gamma$ - and  $\delta$ -Alq<sub>3</sub> share the same isomer [37,40].

Conventional <sup>1</sup>H and <sup>13</sup>C NMR investigations at RT revealed that, regardless of the starting material ( $\alpha$ ,  $\beta$ ,  $\gamma$  or  $\delta$  phases), only the mer-Alq<sub>3</sub> species is present in solution; however, when  $\gamma$ - or  $\delta$ -Alq<sub>3</sub> are suspended in CDCl<sub>3</sub> at  $-50$  °C, the *pure fac-isomer* can be observed. Indeed, fac-Alq<sub>3</sub> is inert at  $-50$  °C for several hours and starts to convert in mer-Alq<sub>3</sub> at  $-20$  °C (see Fig. 11) [37]. Intramolecular ligand scrambling in the mer isomer has been recently studied by dynamic NMR in CDCl<sub>3</sub> solution (283–310–K temperature range) [42]; the activation parameters derived therein for the mer/mer and mer/fac interconversions confirmed either the impossibility to directly observe fac-Alq<sub>3</sub> resonances at room temperature and its inertness at lower temperatures.

Our studies led to the phase transformation diagram reported in Fig. 12 and to the selective production of ‘pure’ polycrystalline  $\delta$ -Alq<sub>3</sub>, the XRPD pattern of which was easily indexed. At this point simulated annealing techniques, in conjunction with the funda-

mental information provided by the variable temperature NMR spectroscopy (see Fig. 11), made it possible to obtain a suitable structural model for the  $\delta$ -Alq<sub>3</sub> phase. After the deposit of our patent [37] and our first attempt to publish these results<sup>7</sup> many other studies on this subject appeared (including an XRPD structural characterization [38], a single crystal X-ray diffraction study [40] and a solid-state <sup>27</sup>Al CP/MAS NMR spectroscopic study [43]), while we faced substantial, perhaps unreasonable difficulties in publishing our results [44].

One may question whether XRPD *alone* would have led to the correct structural model in the absence of ‘external information’ The fortunate availability of two independent XRPD ab initio structural characterizations of the  $\delta$ -Alq<sub>3</sub> phase and of experimental patterns of different origins and quality [37,44] allows us to build Table 2, where subtle, but significant differences can be appreciated.

The results reported in Table 2 clearly show that, in principle, all three experiments may discriminate (with a different degree of certainty) between the two structural hypotheses. However, what is difficult to ascertain is the role of external knowledge during the ‘solution’ process. Indeed, as nicely suggested by Dinnebier [44], “it turned out, that global optimization algo-

<sup>7</sup> Manuscript N° 1075213 sent to Science on 16.06.2002.

Table 2

Comparison of final refinement results for two different stereoisomers and three independent data collections. All computations were performed using TOPAS and rigid bodies hinged about the aluminum atom as described in Refs. [37,40]

	D8-K $\alpha_{12}$		Stoe-K $\alpha_1$		X3B1	
Typical fwhm (°)	0.14		0.14		0.034	
Maximum peak-to-background	147		15		26	
Refined % of $\gamma$ -Alq <sub>3</sub>	5.0		1.4		1.2	
Agreement indices	$R_{wp}$	$R_B$	$R_{wp}$	$R_B$	$R_{wp}$	$R_B$
Fac-Alq <sub>3</sub>	0.071	0.030	0.063	0.020	0.075	0.045
Mer-Alq <sub>3</sub>	0.185	0.105	0.112	0.078	0.134	0.079

*...rhythms in direct space run into severe problems in localizing the global minimum except if the correct isomer is used as starting model allowing the torsion angles to vary within certain limits. Only the high angle part of the powder pattern contains the information which is necessary to distinguish between different isomers. Nevertheless, the correct solution (if found) can be clearly identified.*"

In this particular case, the agreement indices of the *mer*-stereoisomers alone could have easily led to an unfortunate misinterpretation, taking also into account that these values can further be lowered by data massaging, for example by releasing some restraints or by introducing texture or other microstructural effects. Worthy of note, the presence of *one* short intermolecular contact allows to discard the *mer* isomer hypothesis on a stereochemical basis. However, since the intrinsic limitations of the XRPD method may result in a slight misorientation of the refined fragment(s), the presence of such bad contact could also have been tolerated and considered either as: (i) a fake intermolecular contact or, of even more dramatic consequences, (ii) an unduly elongated bond of a new C–C bonded *polymer*, obtained by high-temperature (ca. 400 °C) H<sub>2</sub> elimination<sup>8</sup>.

Thus, since it is only the crystallographer who eventually decides whether or not the 'best available solution' well approximates reality, the larger the external information the easier and reliable the solution will be.

### 3. Conclusions and outlook

The validation of structural results of low quality on adding external observations is a customary behavior

<sup>8</sup> Obviously this would contrast the observation that upon dissolution of  $\delta$ -Alq<sub>3</sub>, followed by solvent removal, pure  $\alpha$ -Alq<sub>3</sub> is retrieved.

in protein crystallography; analogously, combination of EXAFS with PD data has also been reported [45]. All these approaches are ultimately based on the assumption that, if the structural model is optimized vs. data of different origins (diffraction, theory, spectroscopy, database frequencies, etc.), it is likely that systematic errors are cancelled or greatly limited.

The use of MM significantly increases the confidence in the final model; indeed, the coupling of XRPD with MM computations in the crystal lattice can successfully discriminate between a few alternative models by *actively* using experimental, i.e. *accessible*, information on lattice metrics, space group symmetry operations and heavy atom location. This approach, provided that a proper force field is available, is thought to increase the resolution inherent in the diffraction method and, therefore, to act as a lens capable to rescue subtle structural details which XRPD data alone cannot afford. In addition, the use of a joint, or even uncoupled, Rietveld/MM refinement supersedes the common behavior of introducing *arbitrarily weighted* restraints, since it weighs on a *physical basis* the different energetic contributions, leaving, as the only arbitrary choice, the relative importance of the two (partial) cost functions ( $R_{wp}$  and  $E$ ), to be possibly equipartitioned.

In this mini-review we have also shown the importance of tailored experiments (such as SAED, NPD, NLO, NMR and other spectroscopic measurements) which, alone, cannot afford the structural information sought, but which invaluablely assist the development of the 'true' model.

Obviously, single crystal X-ray diffraction still is the most powerful *structural* tool in the organometallic and co-ordination chemist's hands. Without this technique the whole branch of structural physical chemistry, as well as many fields of synthetic chemistry where spectroscopy alone is of little use, would not exist. How-

ever, it would be extremely unfortunate if the stereochemistry of important organometallic species, or of entire classes of compounds, would remain unknown because of the lacking of suitable well-diffracting single crystal specimens.

The number of molecular (or, more generally, *covalent*) structures solved and refined from powder diffraction data are steadily increasing. A quick survey in the most recent CSD release (April 2004) shows indeed about 700 entries under the ‘powder’ flag, 347 of which contain metal atoms<sup>9</sup>. If compared to the pioneering ages, where a handful of structures were solved (yearly) by this method (mostly exploiting the newly available synchrotron sources), we can safely state that the number of scientists using this technique in their daily work has definitely grown, with the obvious consequence that new classes of compounds have been characterized, opening the way to new (and significant) chemistry. However, there is still a gap between the number of actual users of the method and the multitude of chemists which would greatly benefit from it. Thus, in accordance with our original goal, and *particularly after it has been shown that the interplay between experiments of different origins give the highest confidence to the obtained results*, we easily foresee, for structural powder diffraction from conventional laboratory data, a bright, not far, future.

## Acknowledgements

We thank all co-workers who have participated in this project for their continuous support and helpful discussions. Funding from the Italian MURST and CNR is also acknowledged.

## References

- [1] V.K. Pecharsky, P.Y. Zavalij, *Fundamentals of Powder Diffraction and Structural Characterization of Materials*, Kluwer Academic Publishers, Norwell, USA, 2003.
- [2] A. Le Bail, *Powder Diffr.* 19 (2004) 249–254.
- [3] A. Le Bail, *Mater. Sci. Forum* 378 (2001) 65.
- [4] Collectively presented in: W.I.F. David, K. Shankland, L.B. Mc Cusker, C. Baerlocher (Eds.), *Structure Determination from Powder Diffraction Data*, IUCr Monographs on Crystallography 13, Oxford University Press, Oxford, New York, 2002.
- [5] N. Masciocchi (Ed.), *Powder Diffraction of Molecular Functional Materials*, CPD Newsletters No. 31, International Union of Crystallography, May 2004.
- [6] N. Masciocchi, M. Moret, P. Cairati, A. Sironi, G.A. Ardizzoia, G. La Monica, *J. Am. Chem. Soc.* 116 (1994) 7768.
- [7] N. Masciocchi, G.A. Ardizzoia, A. Maspero, G. La Monica, A. Sironi, *Angew. Chem. Int. Ed. Engl.* 37 (1998) 3366.
- [8] N. Masciocchi, M. Moret, A. Sironi, G.A. Ardizzoia, S. Cenini, G. La Monica, *J. Chem. Soc. Chem. Commun.* (1995) 1955.
- [9] N. Masciocchi, A. Sironi, *J. Chem. Soc., Dalton Trans.* (1997) 4643.
- [10] A.C. Larson, R.B. Von Dreele, Los Alamos National Laboratory Report, LAUR 86-748, 2000.
- [11] J. Rodriguez Carvajal, in: XVth Congress of the International Union of Crystallography, Proc. Satellite Meeting on Powder Diffraction, Toulouse, France, 1990, p. 127.
- [12] F. Izumi, T. Ikeda, *Mater. Sci. Forum* 321 (2000) 198.
- [13] A. Kern, A. Coelho, TOPAS V. 3.1, Bruker AXS GmbH, Karlsruhe, Germany, 2003.
- [14] E. Corradi, N. Masciocchi, G. Pályi, R. Ugo, A. Vizi-Orosz, C. Zucchi, A. Sironi, *J. Chem. Soc., Dalton Trans.* (1997) 4651.
- [15] D. Eufri, A. Sironi, *J. Mol. Graph.* 7 (1989) 165.
- [16] P.L. Mercandelli, M. Moret, A. Sironi, *Inorg. Chem.* 37 (1998) 2563.
- [17] N. Masciocchi, F. Ragaini, S. Cenini, A. Sironi, *Organomet.* 17 (1998) 1052.
- [18] F. Ragaini, S. Cenini, *J. Mol. Catal. A: Chem.* 109 (1996) 1.
- [19] N. Masciocchi, R. Bianchi, P. Cairati, G. Mezza, T. Pilati, A. Sironi, *J. Appl. Crystallogr.* 27 (1994) 426.
- [20] A. Immirzi, *Acta Crystallogr.* A34 (1978) S348; B36 (1980) 2378.
- [21] S. Brückner, A. Immirzi, *J. Appl. Crystallogr.* 30 (1997) 207.
- [22] J.K. Bera, K.R. Dunbar, *Angew. Chem. Int. Ed. Engl.* 41 (2002) 4453.
- [23] N. Masciocchi, G. D’Alfonso, L. Garavaglia, A. Sironi, *Angew. Chem. Int. Ed. Engl.* 39 (2000) 4478.
- [24] N. Masciocchi, M. Moret, P. Cairati, F. Ragaini, A. Sironi, *J. Chem. Soc., Dalton Trans.* (1993) 471.
- [25] N. Masciocchi, A. Sironi, S. Chardon-Noblat, A. Deronzier, *Organometallics* 21 (2002) 4009.
- [26] A. Altomare, M.C. Burla, M. Camalli, B. Carrozzini, G.L. Cascarano, C. Giacovazzo, A. Guagliardi, A.G.G. Moliterni, G. Polidori, R. Rizzi, *J. Appl. Crystallogr.* 32 (1999) 339.
- [27] G. Orpen, *J. Chem. Soc., Dalton Trans.* (1980) 2509.
- [28] W.R. Hastings, M.C. Baird, *Inorg. Chem.* 25 (1986) 2913.
- [29] S. Luukkanen, P. Homanen, M. Haukka, T.A. Pakkanen, A. Deronzier, S. Chardon-Noblat, D. Zsoldos, R. Ziessel, *Appl. Catal. A* 185 (1999) 157 and references therein.
- [30] J.M. Rueff, N. Masciocchi, P. Rabu, A. Sironi, A. Skoulios, *Chem. Eur. J.* 8 (2002) 1813.

<sup>9</sup> These values include also pure refinements, without ab initio structure solution. A more indicative figure, although not disaggregated among the different classes of compounds can be found at <http://sdpd.univ-lemans.fr/iniref.html>.

- [31] D.M.P. Mingos, D.J. Wales, *Introduction to Cluster Chemistry*, Prentice Hall, Upper Saddle River, NJ, USA, 1990.
- [32] R.D. Wilson, R. Bau, *J. Am. Chem. Soc.* 98 (1976) 4687.
- [33] B. Nuber, F. Oberdorfer, M.L. Ziegler, *Acta Crystallogr. B* 37 (1981) 2062.
- [34] N. Masciocchi, G. D'Alfonso, W. Kockelmann, W. Schäfer, A. Sironi, *J. Chem. Soc. Chem. Commun.* (1997) 1903.
- [35] C.W. Tang, S.A. Van Slyke, *Appl. Phys. Lett.* 51 (1987) 913.
- [36] M. Brinkmann, G. Gadret, M. Muccini, C. Taliani, N. Masciocchi, A. Sironi, *J. Am. Chem. Soc.* 122 (2000) 5147.
- [37] N. Masciocchi, A. Sironi, M. Muccini, M.A. Loi, Italian Patent MI2002A001330, 14.06.2002 (with PCT extension).
- [38] (a) M. Cölle, R. Dinnebier, W. Brütting, *J. Chem. Soc. Chem. Commun.* (2002) 2908; (b) M. Rajeswaran, T.N. Blanton, K.P. Kublek, *Z. Kristallogr. NCS* 218 (2003) 439.
- [39] M. Rajeswaran, T.N. Blanton, K.P. Kublek, *Z. Kristallogr. NCS* 218 (2003) 439.
- [40] M. Muccini, M.A. Loi, K. Keveney, R. Zamboni, N. Masciocchi, A. Sironi, *Adv. Mater.* 16 (2004) 861–864.
- [41] M. Braun, J. Gmeiner, M. Tzolov, M. Cölle, F. Meyer, W. Milius, H. Hillebrecht, O. Wendland, J. von Schütz, W. Brütting, *J. Chem. Phys.* 114 (2001) 9625.
- [42] M. Utz, C. Chen, M. Morton, F. Papadimitrakopoulos, *J. Am. Chem. Soc.* 125 (2003) 1371.
- [43] M. Utz, M. Nandagopal, M. Mathai, F. Papadimitrakopoulos, *Appl. Phys. Lett.* 83 (2003) 4023.
- [44] Data from R. Dinnebier's site: <http://www.mpi-stuttgart.mpg.de/xray/html/download.html>.
- [45] N. Binsted, M.J. Pack, M.T. Weller, J. Evans, *J. Am. Chem. Soc.* 118 (1996) 10200.